Turkish Journal of Earth Sciences (Turkish J. Earth Sci.), Vol. 19, 2010, pp. 79–100. Copyright ©TÜBİTAK
doi:10.3906/yer-0807-3 First published online 28 December 2009

Surface and Subsurface Characteristics of the Çankırı Basin (Central Anatolia, Turkey): Integration of Remote Sensing, Seismic Interpretation and Gravity

NURETDİN KAYMAKCI[1], ŞENOL ÖZMUTLU[2], PAUL. M. VAN DIJK[3] & YAKUP ÖZÇELİK[4]

[1] RS/GIS Labaoratory, Department of Geological Engineering, Middle East Technical University, TR–06531 Ankara, Turkey (E-mail: kaymakci@metu.edu.tr)

[2] Vryhof Anchors B.V. Rhijnspoor 255 2901 LB - PO Box 109 2900 AC, Capelle a/d IJssel, The Netherlands

[3] ITC, Hengelosestr 99, P.O. B0x 6, 7500 AA Enschede, The Netherlands

[4] Turkish Petroleum Coorporation (TPAO), Söğütözü Caddesi No: 27, Söğütözü, TR–06520 Ankara, Turkey

Received 03 July 2008; revised typescript receipt 02 March 2009; accepted 04 March 2009

Abstract: The geology of the Çankırı Basin has been studied using multi-source data including satellite images, aerial photos, gravimetric data and seismic sections, which are subsequently used to generate maps and a 3D model of that part of the basin covered by the seismic sections. From the compilation, three different phases of deformation are recognized. The earliest phase is characterized by thrusting during the Early Tertiary. The second deformation phase is characterized by extensional deformation associated with normal faulting in the latest Early Miocene to Middle Miocene. The third, and the last, phase is characterized by compressional deformation manifested by inversion of some of pre-existing normal structures that has been taken took place since the Late Miocene. Finally, the constructed model and the maps helped to better understand the 3D geometry and tectono-sedimentary evolution of the Çankırı Basin and the collisional history of the Sakarya Continent and the Kırşehir Block along the İzmir-Ankara-Erzincan Suture Zone.

Key Words: Remote Sensing, data integration, subsurface geology, seismic interpretation, gravity, Çankırı Basin, central Anatolia

Çankırı Havzası'nın Yüzey ve Yeraltı Jeolojisi (Orta Anadolu, Türkiye): Uzaktan Algılama, Sismik Yorumlama ve Gravite Verilerinin Entegrasyonu

Özet: Çankırı Havzasının jeolojisi uydu görüntüleri, hava fotografları, gravite ve sismik kesitleri içeren çok kaynaklı veri setleri kullanılarak çalışılmış ve elde edilen veriler havzanın değişik amaçlı haritaların hazırlanması ve sismik kesitlerin kapladığı kısmının ise 3 Boyutlu modelinin oluşturulmasında kullanılmıştır. Derlenen verilerden havzanın üç farklı evrede deformasyona uğradığı anlaşılmıştır. Erken Tersiyer dönemine tarihlenen en eski evre bindirme fayları ile karakterizedir. Erken Miyosen sonu ile Orta Miyosen dönemine tarihlenen ikinci evre, normal faylanma ile ilişkili genişleme tektoniği ile karakterizedir. Geç Miyosen'den itibaren etkin olan üçüncü ve son evre ise bir önceki evrede gelişmiş normal fayların terslenmesi ile kendini gösteren, sıkıştırmalı deformasyon ile karakterizedir. Sonuç olarak, oluşturulan model ve haritalar, havzanın 3 Boyutlu geometrisi ile tektono-stratigrafik evrimi ve İzmir-Ankara-Erzincan Kenet Kuşağı boyunca meydana gelen Sakarya Kıtası ile Kırşehir Bloğunun çarpışma tarihçesinin daha iyi anlaşılmasını sağlamıştır.

Anahtar Sözcükler: Uzaktan Algılama, veri entegrasyonu, yeraltı jeolojisi, sismik yorumlama, gravite, Çankırı Havzası, Orta Anadolu

Introduction

The Çankırı Basin, one of the largest Tertiary basins in Turkey (Figure 1), has possible economic hydrocarbon and industrial mineral (mainly evaporatic) reserves. It lies within the İzmir-Ankara-Erzincan Suture Zone (IAESZ) (Figure 1), which demarcates the former position of the northern branch of the Neotethys Ocean. After consumption of Neotethys, final collision occurred along the IAESZ, during which the Sakarya continent of the Pontides in the north amalgamated with the Kırşehir Block in the south (Şengör & Yılmaz 1981; Görür *et al.* 1984; Robertson & Dixon 1984; Tüysüz & Dellaloğlu 1992; Okay *et al.* 1998; Robertson *et al.* 1996; Kaymakcı 2000; Kaymakcı *et al.* 2000, 2003a, b). The Çankırı Basin is a unique area in north central Anatolia to study subduction and collision processes owing to an almost 4-km-thick Upper Cretaceous to recent in-fill, with only minor breaks in sedimentation.

The number of published geological studies in the Çankırı Basin is relatively small. This is due to difficulty in dating continental deposits as well as the geological complexity of the region, with a superimposed, multi-deformational history. Recently, due to advances in digital technology and improvements in geophysical and remote sensing methods, the number of studies in the region has increased. For this purpose, the Turkish Petroleum Co. (TPAO, Ankara-Turkey) shot 24 seismic lines, which amount to nearly 1000 km in line length. Improved gravity measurements were made available by the General Directorate of Mineral Exploration and Research Department (MTA, Ankara-Turkey).

The aim of this paper is to present the surface and subsurface characteristics of the Çankırı Basin based on satellite and airborne remote sensing, seismic images, local gravity, and field studies in order to understand better the subduction history of the Neotethys and collisional and post collisional processes along the İzmir-Ankara-Erzincan Suture zone. The remotely sensed data, combined with field data and the published literature, were used to obtain an up-to-date geological map of the basin. The seismic sections were interpreted and were used to construct a 3D model for part of the basin. The gravity data were used to obtain gravity anomaly images that were used to validate the generated 3D model.

Geological Background

The Çankırı Basin is located between the Sakarya Continent in the north and the Kırşehir Block in the south and is bounded in the west, north and east by an ophiolitic mélange (North Anatolian Ophiolitic Mélange, NAOM, cf. Rojay 1995), associated with Upper Cretaceous volcano-sedimentary rock assemblages, which collectively constitute the rim of the basin (Figure 1). The same rock assemblages partly underlie the infill of the Çankırı Basin in the north, and in the south it is underlain and delimited by the Sulakyurt granitoids, forming the northernmost tip of the Kırşehir Block.

The infill of the Çankırı Basin accumulated in 5 different cycles of sedimentation (Figure 2). The oldest cycle comprises Upper Cretaceous to Paleocene volcaniclastic rocks (Yaylaçayı and Yapraklı formations), regressive shallow marine units and Paleocene mixed environment red clastics and carbonates (Dizilitaşlar, Kavak and Badiğin formations). In this paper, these are referred to as the '*Upper Cretaceous units*'. They are overlain by the second cycle, which is a Paleocene to Oligocene regressive flysch to molasse sequence referred to as the '*Tertiary clastics*' in this study. In it a widespread thin (<100 m) '*nummulitic limestone*' of Middle Eocene age (Kocaçay Formation), that constitutes the marker horizon in the seismic sections, passes upwards into very thick (up to 2000 m) Middle Eocene to Oligocene continental red clastics (İncik Formation) interfingering with and overlain by Oligocene evaporites (Güvendik Formation). The third cycle is represented by fluvio-lacustrine clastics deposited in the Early to Middle Miocene, which, together with the Tortonian Tuğlu Formation are referred to as the '*Middle to Upper Miocene units*' in this study. The fourth cycle is represented by upper Miocene fluvio-lacustrine deposits which frequently alternate with evaporites (Tuğlu, Süleymanlı and Bozkır formations). Plio–Quaternary alluvial fan deposits and recent alluvium locally overlie all these units (Figure 2).

The structures, which have played a role in the tectonic development of the Çankırı Basin, from

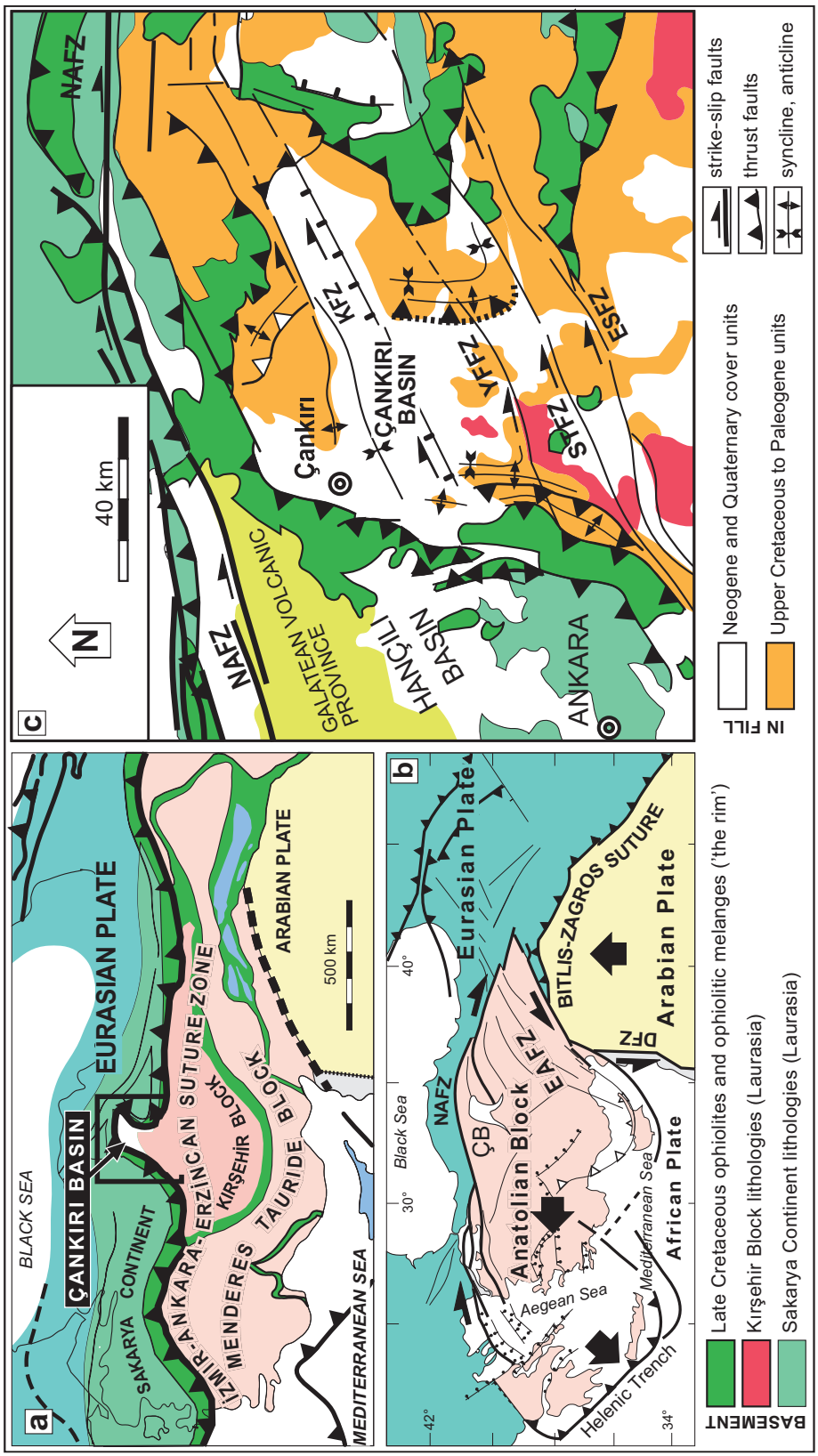

Figure 1. (**a**) Inset map showing the geological outline of Eastern Mediterranean area (modified after Şengör *et al.* 1984; Okay *et al.* 1998). Box shows the location of the study area. (**b**) Active tectonic scheme of the Eastern Mediterranean area. ÇB– Çankırı Basin, DFZ– Dead Sea Fault Zone, NAFZ– North Anatolian Fault Zone (Şengör *et al.* 1985; Barka 1992; Özçelik 1994; Kaymakcı 2003a). (**c**) Tectono-stratigraphic map of central Anatolia. ESFZ– Ezinepazarı-Sungurlu Fault Zone, KFZ– Kızılırmak Fault Zone, YFFZ– Yağbasan-Faraşlı Fault Zone.

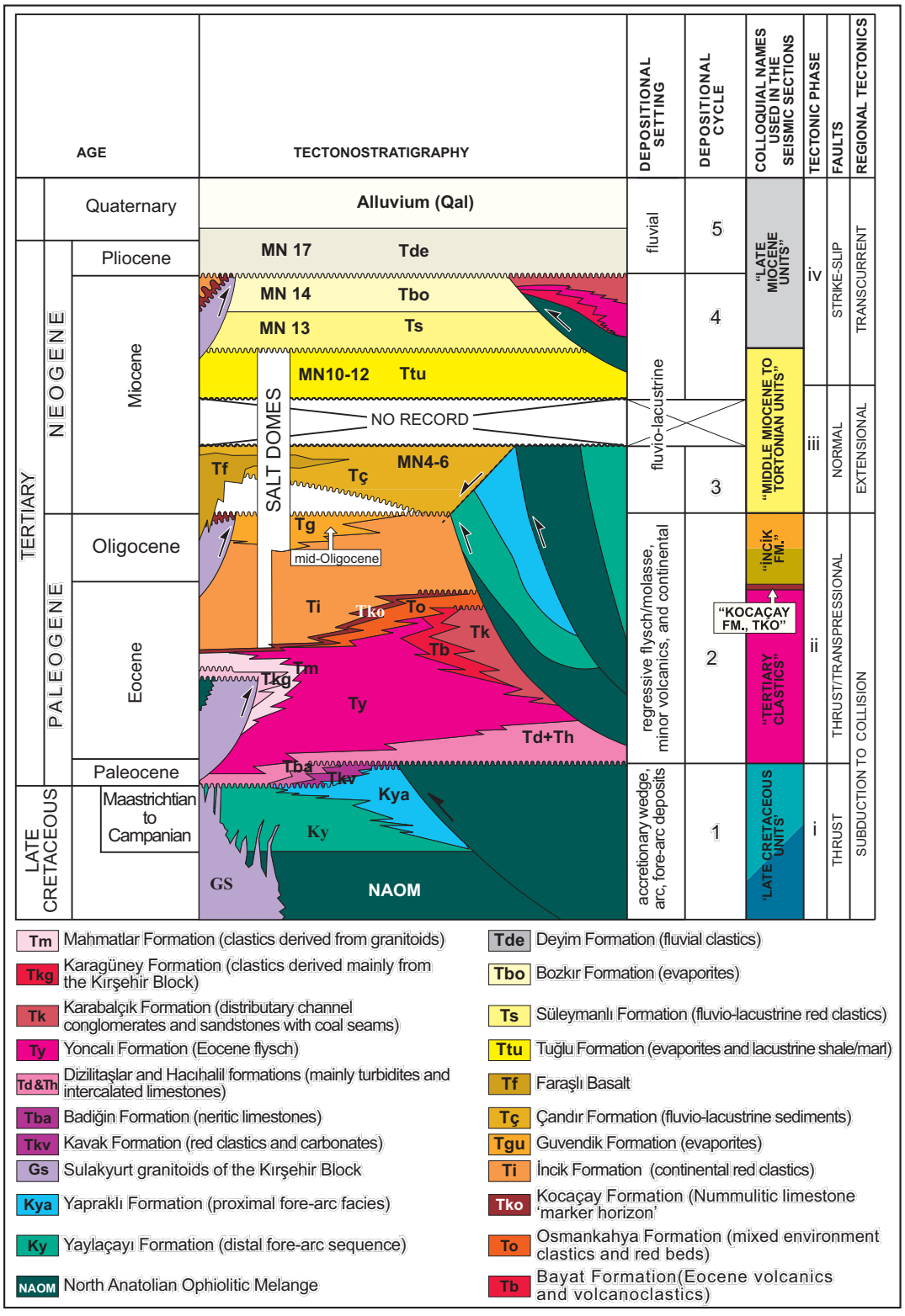

Figure 2. Generalized tectono-stratigraphic column of the units exposed in and around the Çankırı Basin. MN– ages of units in European mammal zones.

oldest to youngest, are: (1) Compressional faults (thrust and reverse faults with locally considerable amounts of strike-slip component) situated mainly along the rim of the basin. (2) Dominantly NE–SW-oriented strike-slip faults that cut the basin infill, the basement, and the rim. These include the presently active Sungurlu Fault Zone (a sub strand of the Ezinepazarı-Sungurlu Fault Zone), the Yağbasan-Faraşlı Fault Zone and the Kızılırmak Fault Zone (Figure 1c). (3) Other, but less pronounced structures are normal faults concentrated mainly in the central part of the basin and which have displaced some of the compressional structures at the rim (Figure 3).

The active tectonics of the Çankırı Basin area are currently dominated by regional transcurrent tectonics (Figure 1c), controlled by splay faults of the North Anatolian Fault Zone (NAFZ). The NAFZ is an approximately 1200-km-long strike-slip fault zone that formed due northwards drift of the Arabian Plate and its collision with the Eurasian Plate (Şengör & Yılmaz 1981; Jackson & McKenzie 1984; Şengör *et al.* 1985).

Remote Sensing

Two scenes from Landsat Thematic Mapper (TM)-5 images were used as a basis for the geological map of the Çankırı Basin (Figures 3 & 4). The characteristics of these images are given in Table 1. Before the images were processed, a radiometric enhancement (Lavreau 1992; Richard 1993) was carried out and then they were mosaiced. Subsequently, the portion of the image covering the Çankırı Basin was extracted from the mosaic for further analysis.

A number of different image enhancement techniques were performed to differentiate and map each lithostratigraphic unit and to delineate the geological structures. These techniques include simple linear contrast enhancement, decorrelation stretch enhancement (Soha & Schwartz 1978; Gillespie *et al.* 1986), Intensity-Hue-Saturation enhancement (Hayden 1982; Daily 1983; Grasso 1993) and Principal Component Analysis (Taylor 1974; Chavez & Kwarteng 1989). Since each technique has its own strengths and weaknesses, they could only enhance certain types of geological units and none of the techniques had the ability to discriminate all of the lithological units and structures in one scene. Therefore, during interpretation, all the above-mentioned enhancements were used to identify the units and structures in a GIS medium. However, decorrelation stretching technique with band combination of Red: 5, Green: 3, and Blue: 1 produced the optimum enhanced image to show most of the structures and almost all units. Therefore, final interpretation and tracing of the boundaries and plotting of structures were performed on this image while the other processed images were used in support. The image and the resultant map are presented in Figures 3 and 4.

Image Interpretation

The interpretation of the images and the aerial photos was performed in three successive steps. In the first step before fieldwork, published maps were used to support interpretation (Akyürek *et al.* 1980; Dellaloğlu *et al.* 1992; Özçelik & Savun 1993; Özçelik 1994). The resulting interpreted map was verified during field studies. In areas where sufficient resolution could not be achieved, due to the small scale of the structures and/or the intensity of the deformation, field mapping was performed using 1:25.000 scale topographical maps. Then the images were re-interpreted and verified in the successive fieldwork seasons. This procedure (Figure 5) was repeated four times and verified in the field until a final map was produced. In the final map (Figure 4), the formation boundaries, faults, folds and the photo-lineaments (O'Leary *et al.* 1976) were traced using on-screen digitizing directly onto the image using advanced cartographic techniques. Hardcopies were only utilized during field verification.

Using remote sensing and field data, twenty-eight formations, plus the alluvium, were recognized and mapped (Figure 4). Six of these formations are recognized for the first time in this study. These are, in stratigraphic order, upper Cretaceous quartz-latite member of the NAOM, upper Cretaceous to Paleocene Kavak and Badiğin formations, the Middle Eocene to Oligocene İncik Formation, which was separated into two units (Ti1 and Ti2) although

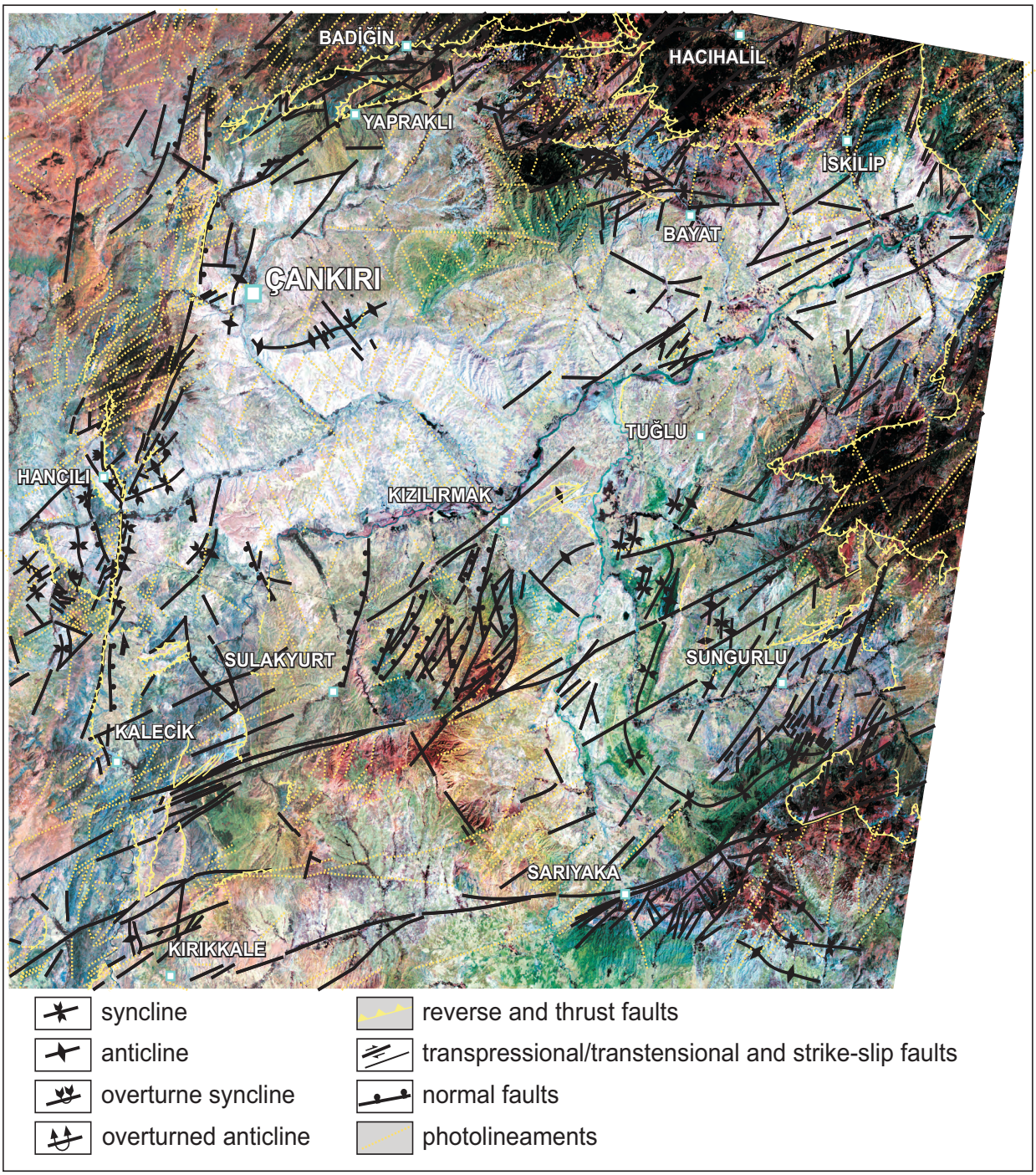

Figure 3. **(a)** Decorrelation stretching enhancement applied Landsat TM-4 Image of the study area (RGB: 5, 3, 1). Major faults, folds and photo-lineaments are overlaid on the image.

in the field they could not be differentiated clearly, the Oligocene Güvendik Formation and Tortonian Tuğlu Formation, which had previously been mapped as a single unit. In addition, the Kılçak, Altıntaş, Hancılı, and Çandır formations, which were partly recognized by previous researchers, have been separated and mapped out for the first time in this study.

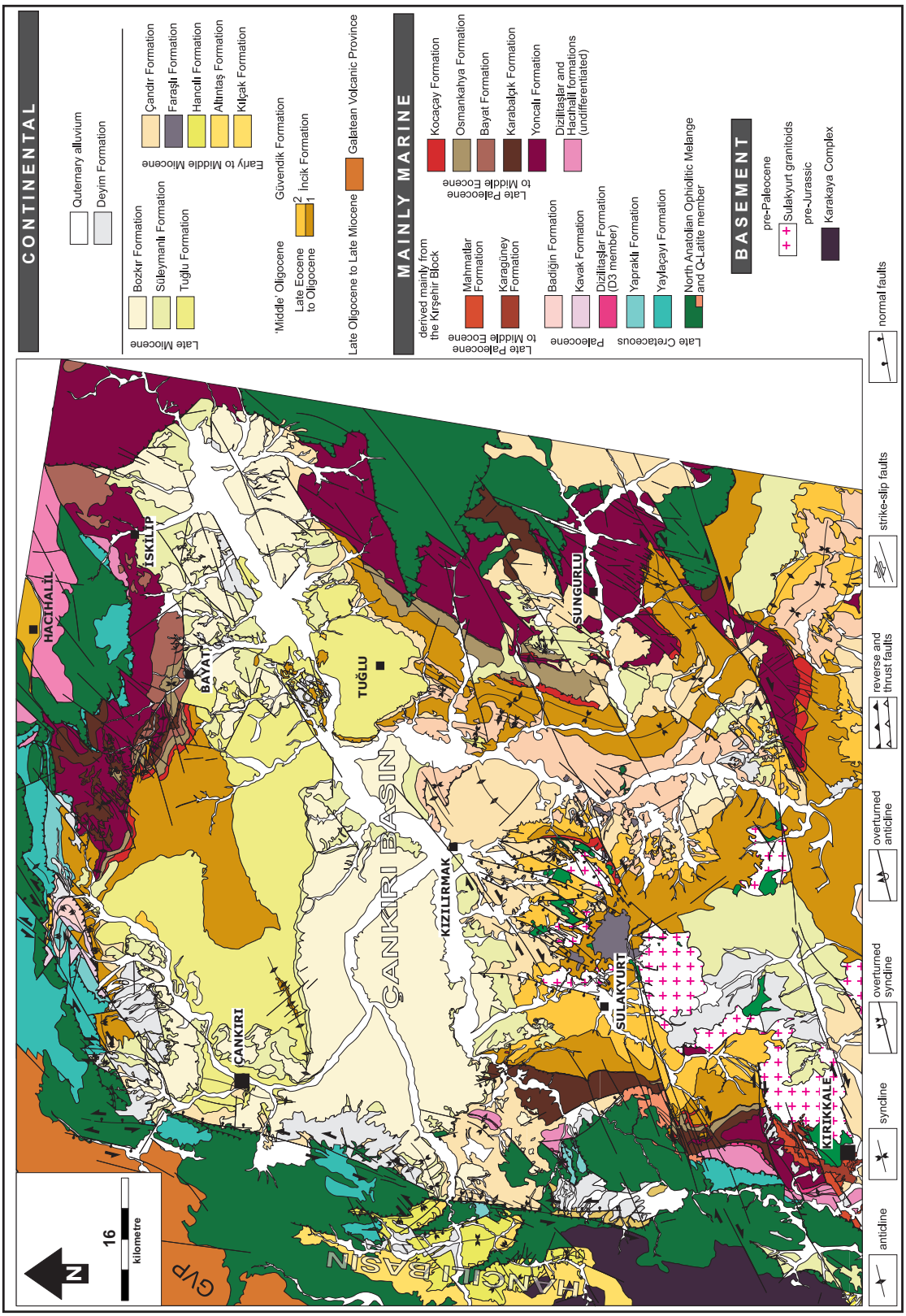

Figure 4. Geological map of the Çankırı Basin.

Table 1. Specifications of the images used in this study.

IMAGE	*LANDSAT TM-5*
Path/row	176/32 and 177/32
Date	17 August 1991 and 01 September 1984
Area covered (x,y)	10800km^2
Coordinates of studied portion (UTM ZONE 36)	
Upper left corner x	523298
Upper left corner y	4523570
Lower right corner x	630518
Lower right corner y	4422840
Aerial Photos	
Colour	Black and white
Date	1963-1974
Scale	1:60.000 full coverage 1:35.000 partial coverage (mainly basin margins are covered)

Lineament Analysis

Photo-lineaments are defined as simple or composite linear features on the earth's surface which can be recognized on maps or on satellite images, must be mappable for at least a few kilometres length and which have a rectilinear or slightly curvilinear geometry and presumably reflect subsurface phenomena (O'Leary *et al*. 1976; Park & Jaroszewski 1994). These lineaments (Figure 6) were categorized into two classes based on their quality. Only those with appreciable offset are classified as 'faults' and were analyzed together with the faults that are verified in the field (see Kaymakcı *et al*. 2000, 2003a). The others are classified as photo-lineaments. In the analyses, the Çankırı Basin was divided into 11 sub-areas (Figure 6), based on variation in structural trends and the geometry of the basin rim. For each sub-area, length weighted rose diagrams for the faults and the photo lineaments were prepared and compared.

Spatial Characteristics of the Lineaments

Apart from the differences in the orientations of the lineaments, there is also a difference in their distribution in the study area. The lineaments are concentrated mainly in the rim of the basin and in the pre-Neogene units. The southern sub-areas (sub areas 3, 4, 5 and 9) have the highest frequency of faults, while the western sub-areas (sub areas 1 to 3) have the highest frequency of photo-lineaments (Tables 2 & 3). Sub-area 7 has the least frequency of faults, and, considering its size, the photo-lineaments are also fewer than in other parts of the Çankırı Basin (Figure 6).

Tectonic Implications of the Lineaments

The domination of the lineaments within the pre-Neogene units may indicate that these units were subjected to deformation phases (Kaymakcı *et al.* 2000, 2003a) that did not affect the Neogene units. It is obvious that the younger rocks are exposed to fewer deformation phases, as in sub-area 7 where mainly Late Miocene formations are exposed.

The rose diagrams prepared for all the faults and for the photo-lineaments display a Riedel geometric pattern (Figure 9b) in which all components of the Riedel shears are developed and displayed. In this pattern the Sungurlu, Kızılırmak, and Yağbasan-Faraşlı fault zones constitute the y-shears. The Eldivan Fault Zone (EFZ), which defines the western margin of the Çankırı Basin (sub-areas 1–3), is almost parallel to the orientation of the expected compressional structures (f in Figure 7) in a Riedel system, although, it slightly deviates from it (approximately 15° anticlockwise).

Gravity

The gravity data from the Çankırı Basin and adjacent areas was obtained from MTA (General Directorate of Mineral Exploration and Research (MTA), Ankara-Tukey). The data set has a 2*2 km average sample interval. It was gridded using the conventional Krigging method. The resulting image of the processed gravity data is illustrated in Figure 8.

In the processed gravity image, the rim of the basin, the granitoids of the Kırşehir Block, and two buried (blind) thrust belts (discussed below; one in the central northern part and one in the eastern margin), are expressed respectively as a positive anomaly with respect to the basin in-fill (Figure 8). In addition, a NE–SW-trending fault that dextrally displaces the northern margin of the Çankırı Basin is

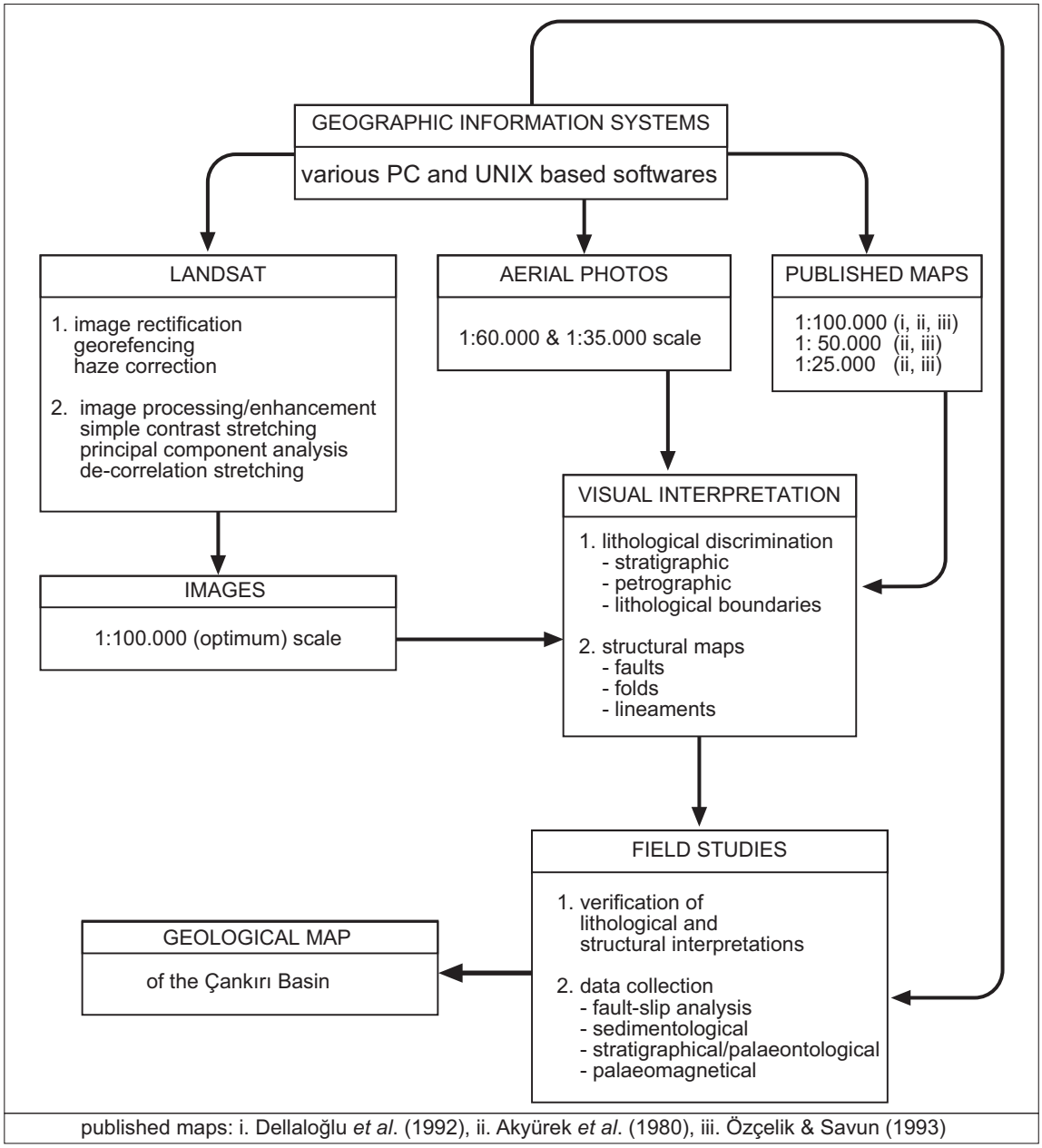

Figure 5. Flow chart illustrating the steps followed in production of the geological map of the study area. Numbers i-iii indicate the references of the published maps. (i) Dellaloğlu *et al*. (1992), (ii) Akyűrek *et al*. (1980), (iii) Őzçelik & Savun (1993).

recognized. This fault is seen only in the pre-Neogene units (Figures 4 & 6) but can be traced below the cover of Neogene units for a considerable distance (approximately 30 km) on the processed gravity image. In the southern part of the basin, the Yağbasan-Faraşlı Fault Zone and the main strand of the Sungurlu Fault Zone (YFFZ and MSFZ, respectively) are delineated on the gravity image (Figure 8). Pseudo-stereo shaded relief images facilitate 3-D visualization of thickness variation of the infill and help the identification of the structures, chiefly including the outline of the rim, the

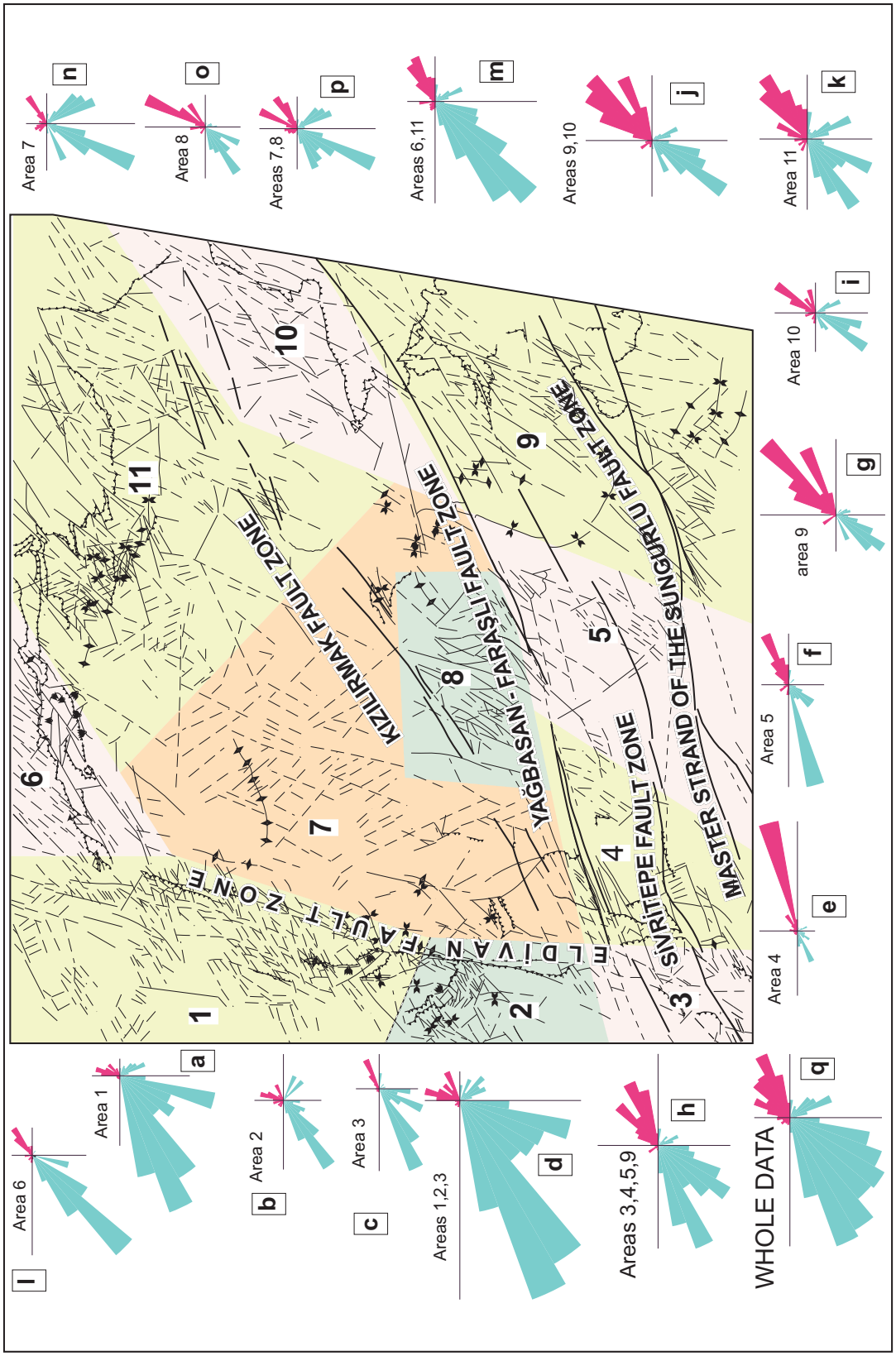

Figure 6. Lineament map of the study area. **(e–w)** rose diagrams for each selected subarea and combinations. The upper quadrants of the rose diagrams display the fault classes and lower quadrants display the photo-lineament classes (see Tables 2 & 3 for the frequencies).

Table 2. Percentages of the faults in the subareas.

	west									east									
Area	80-89 W	←							0-9 W	1-10 E	→							81-90 E	Total Length
1	0	3	1	1	3	0	3	0	2.86	17.1	23	14	6	14	4.3	7.1	0	0	9.78
2	0	4	7	4	4	0	0	0	0	10.7	25	18	4	7	0	18	0	0	3.91
3	0	5	0	0	5	0	0	0	4.76	0	0	0	5	10	24	48	0	0	2.93
4	0	0	2	0	2	0	0	2	0	4.08	2	0	2	4	10	4.1	61	6.12	6.84
5	5.405	0	0	0	0	5	3	1	0	0	0	3	0	9	15	30	18	10.8	10.34
6	6.667	3	2	5	0	0	0	0	6.67	0	0	0	3	22	30	8.3	5	8.33	8.38
7	0	2	0	0	6	5	8	6	3.17	0	5	0	3	8	21	25	8	0	8.80
8	0	0	0	5	0	2	2	3	9.68	1.61	6	42	3	5	18	3.2	0	0	8.66
9	0	0	0	0	1	4	1	0	0	1.39	4	13	15	28	6.9	20	6	0	20.11
10	0	6	0	4	0	0	0	6	3.92	0	6	16	27	0	9.8	5.9	14	1.96	7.12
11	0	3	5	2	1	4	2	2	6.38	2.13	2	1	2	3	11	28	14	10.6	13.13
1,2,3	0	3	3	2	3	0	2	0	2.52	12.6	19	13	5	12	6.7	17	0	0	16.62
3,4,5,9	1.389	0	0	0	1	3	1	1	0.35	1.39	2	7	8	18	11	22	18	3.82	40.22
9,10,	0	2	0	1	1	3	1	2	1.03	1.03	5	13	18	21	7.7	16	8	0.51	27.23
6.11	2.597	3	4	3	1	3	1	1	6.49	1.3	1	1	3	10	18	20	10	9.74	21.51
7.8	0	1	0	2	3	3	5	5	6.4	0.8	6	21	3	6	19	14	4	0	17.46
																			Bulk= 28.81

Table 3. Percentages of the photo-lineaments in the subareas.

	west									east									
Area	80-89 W	←							0-9 W	1-10 E	→							81-90 E	Total Length
1	1	0	1.4	1	2	3	3.6	1	0.6	3.4	13	7	8.4	6	16	19.2	14	0	28.25
2	0	0	8.4	2	8	1	0	0	0	5.263	3	7	6.3	15	25	13.7	4	0	5.37
3	4.8544	0	0	0	2	1	0	2	0	9.709	6	15	7.8	5	19	27.2	1	0	5.82
4	0	0	2.9	1	0	4	8.7	2	0	3.846	6	6	11	7	2.9	25	10	11.54	5.88
5	5.8824	0	0	0	3	0	0	0	0	0.98	3	6	12	12	6.9	5.88	41	3.922	5.76
6	0	0	0	2	0	0	0	0	0	0	11	1	19	36	22	8.33	0	1.042	10.85
7	2.3121	0	1.2	3	9	10	12	1	0	2.312	9	22	12	3	0.6	9.25	0	2.312	9.77
8	1.9417	0	0	0	2	3	2.9	3	4.854	0	1	16	7.8	14	23	11.7	10	0	5.82
9	0	0	0	0	3	0	4.8	6	2.885	4.808	9	15	22	18	1.9	10.6	0	1.923	5.88
10	0	0	0	0	0	6	10	4	0	3.896	18	14	23	3	7.8	6.49	0	2.597	4.35
11	5.0691	2	1.4	1	2	5	8.8	4	0.922	2.765	3	13	8.3	7	15	11.1	7	0.922	12.26
1,2,3	1.4327	0	2.1	1	3	2	2.6	1	0.43	4.585	10	8	8	7	17	19.6	10	0	39.44
3,4,5,9	2.6634	0	0.7	0	2	1	3.4	2	0.726	4.843	6	10	13	10	7.7	17.2	13	4.358	23.33
9,10,	0	0	0	0	2	3	7.2	5	1.657	4.42	13	15	23	12	4.4	8.84	0	2.21	10.23
6.11	2.6895	1	0.7	1	1	3	4.6	2	0.489	1.467	7	7	13	21	18	9.78	4	0.978	23.11
7.8	2.1739	0	0.7	2	7	8	8.7	2	1.812	1.449	6	20	10	7	9.1	10.1	4	1.449	15.59
																			Bulk= 71.19

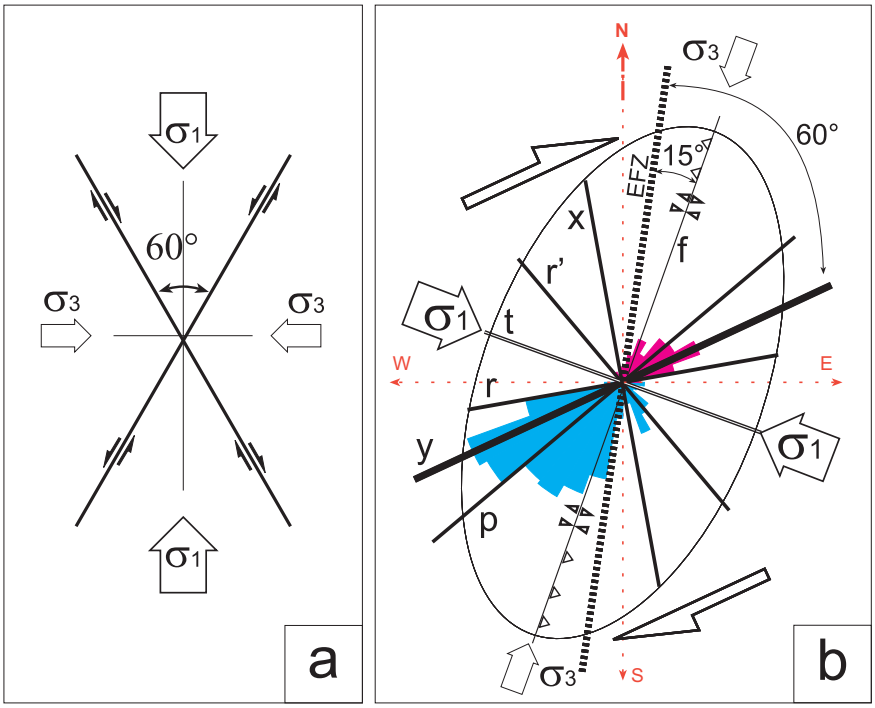

Figure 7. **(a)** Figure illustrating Andersonian geometric relationship between principal stresses (σ_1–σ_3) for brittle faults and the dihedral angle between the faults that would develop under the indicated stress orientations (σ_2 is perpendicular to the plane of the figure), **(b)** Riedel pattern of deformation applied to the Çankırı Basin and respective stress orientations (model is adopted from Bartlett *et al.* 1981; Sylvester 1988; Dresen 1991). These are not listed in reference list. Note the angle between the Eldivan Fault Zone (EFZ) and the σ_1. f– folds and high angle thrust faults, p– secondary synthetic shear, r– synthetic shear, r'– antithetic shear, t– extension structures, y– principal displacement zone.

Yağbasan-Faraşlı Fault Zone (YFFZ), the master strand of the Sungurlu Fault Zone (MSFZ) and a basement step in the Eastern Margin of the Kırşehir Block (Figure 8b, c). The basin fill was found to be the thickest along a NE-trending belt in the northeastern part of the basin. In addition, it was observed that the eastern boundary of the Kırşehir Block is a steeply dipping discontinuity, which we interpreted as a normal fault on the seismic sections.

Three Dimensional (3D) Volume Model

Introduction

3D modelling characterizes the subsurface geology in three dimensions. The process consists of identification of geological entities (i.e. formation boundaries, unconformities, faults, etc.) and their interpolation. The flexibility and 3D visualization capabilities of the interface allow the interpreter to visually analyze data in any direction and decide on the continuity and extrapolation of geological units and discontinuities in 3D. This in turn improves the interpretation of geological features in 3D in the area of interest. In this study, the geometrical functionality of the LYNX software (Lynx Geosystems Incorporation 1997) was used. The geometrical modelling can simply be defined as the definition and interpretation of the boundaries of geological objects.

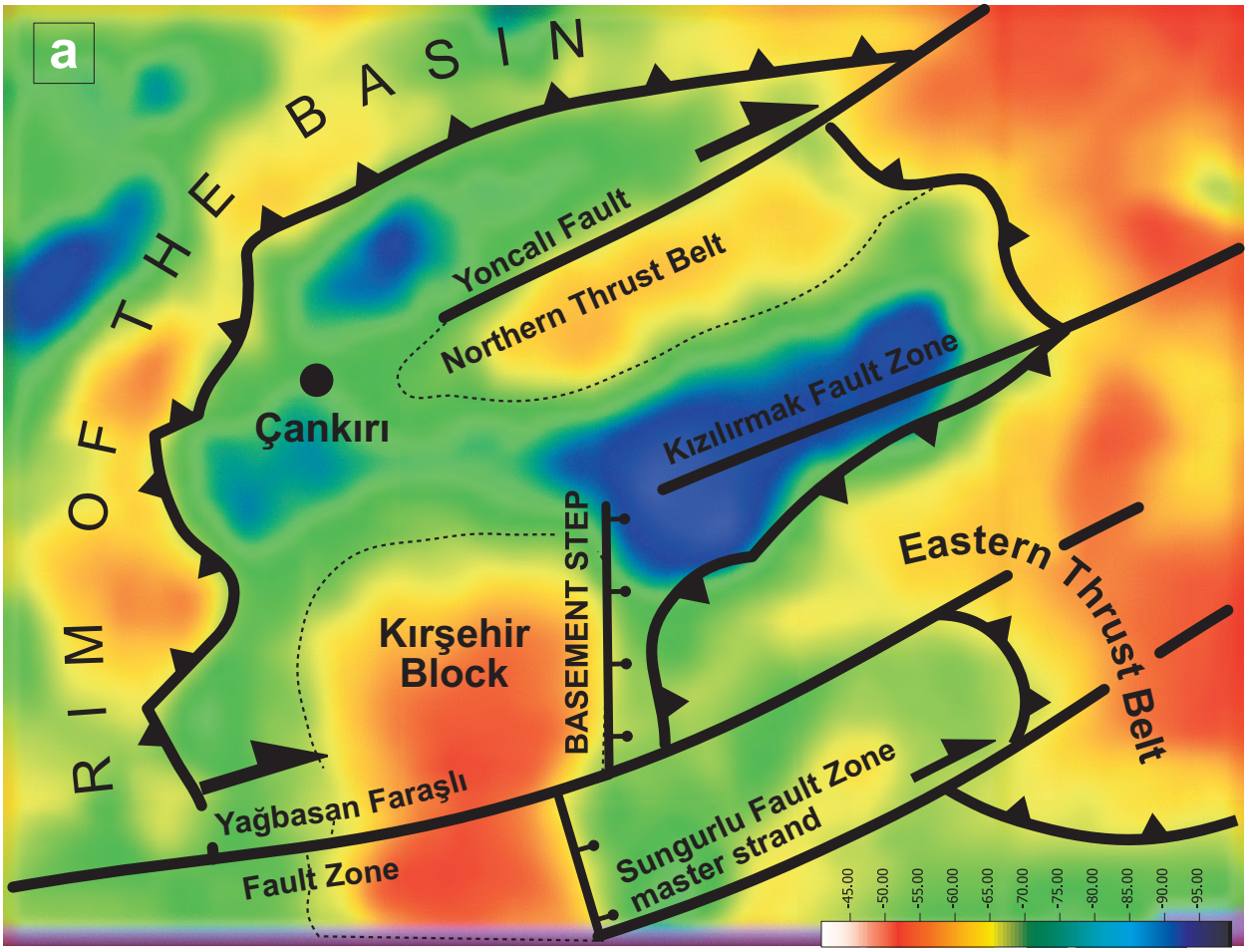

ILLUMINATION ANGLE 315°N/55°

ILLUMINATION ANGLE 315°N/45°

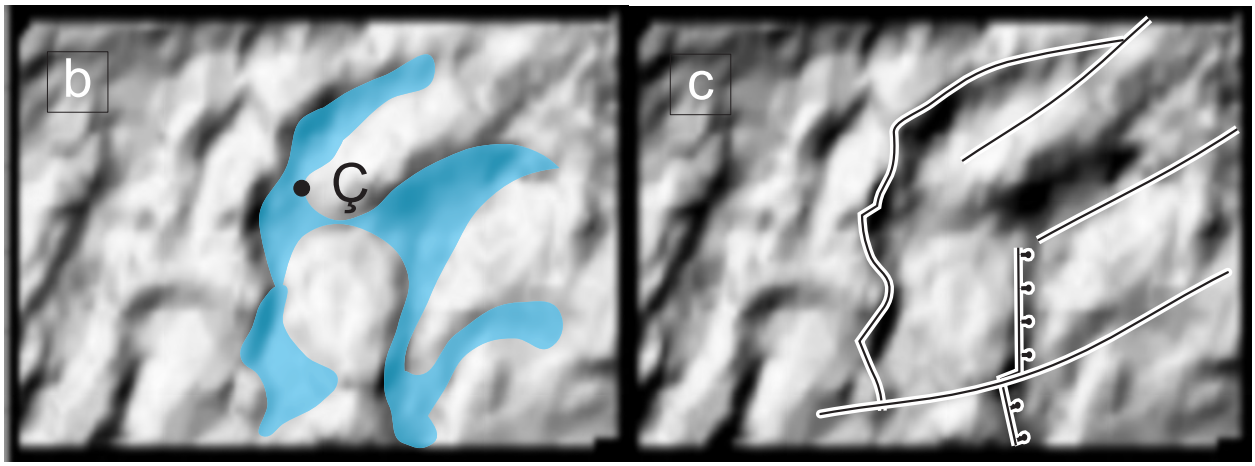

Figure 8. **(a)** Gravity image of the study area obtained from gridding using Krigging of 2*2 km gravity data. Ç– Çankırı. **(b, c)** Pseudo-stereo pair of the shaded relief images of the gravity data. The blue indicates areas where the sediment thickness is the thickest.

Methodology

The data available for 3D modelling consists of geological cross-sections based on 2D seismic sections and geological map. The seismic sections were acquired in three periods between 1988 and 1996 and were processed, stacked and interpreted by the TPAO-Exploration Department (Ankara, Turkey). Unfortunately, no depth conversion was possible due to insufficient borehole information. The orientations of the seismic lines are given in Figure 9a.

Interpretations of the seismic sections were done manually, that is visual interpretation directly from the hard-copies, on the time sections. The interpreted sections were then correlated with the geological map to identify the litho-stratigraphic units. The boundaries of exposed units on the map were extrapolated in the seismic sections and these were subsequently re-interpreted. The final interpretations were digitized using a Calcomp ISO-A0-sized tablet digitizer. The digitized sections were subsequently introduced to the LYNX-software and georeferenced. In order to generate 3D model of the area of interest, regularly spaced parallel sections are required (Figure 9). To do this, volume models with a finite lateral extent were generated for each of the seismic section independently (Figure 10). These volume models were then projected onto the plane of the intermediate section. For the construction of each intermediate section, the volume models of the closest seismic sections were used (Figure 9). In the next intermediate section, the volume model of the previous seismic sections, the first developed intermediate section and the next seismic sections were projected on to the active visualization panel. After this, the next intermediate section was interpreted and used to improve the previous intermediate sections. Transverse sections were then generated and used to improve the interpretation of the previous intermediate sections. This procedure was repeated iteratively until the final regularly spaced mesh of fence diagrams of the region was generated (Figures 10 & 12). Finally, a number of depth maps were derived at 3.50s (second), 2.25s, and 0.50s time levels (Figure 11) for comparison with the surface geological map and the gravity anomaly map.

Results

In the seismic sections, 9 different rock packages were identified (Figure 10a) namely, from older to younger: (1) lithologies of the Kırşehir Block and the upper Cretaceous to Paleocene units (here referred to as 'upper Cretaceous units'); (2) 'Tertiary clastics'; (3) an lower to Middle Eocene nummulitic limestone marker horizon (Kocaçay Formation); (4) 'salt domes' including adjacent deformed rocks; (5, 6) the very thick Middle Eocene to Oligocene 'İncik Formation' is differentiated into two sub units, namely a lower and upper unit; (7) Oligocene 'Güvendik Formation'; (8) 'Middle Miocene to Tortonian' units (Çandır-Tç and Tuğlu-Ttu formations); (9) 'Late Miocene units' (Süleymanlı and Bozkır formations) together with Plio–Quaternary units including alluvium. In addition, in the lower parts of some of the seismic sections, a very distinct reflection horizon was observed (indicated with arrow in Figure 10a). However, this reflector could not be correlated with any exposed lithologies or bore-hole data from the Çankırı Basin. In addition, the interface between the northern tip of the Kırşehir Block and the Late Cretaceous units was not distinguishable (indicated with '?' in the Figure 10a). This might indicate that the Kırşehir Block extends further to the north beyond the seismic coverage area or, due to seismic attenuation, the interface is obscured.

The most spectacular structures in the seismic sections are the northern and eastern fold and thrust belts, a step (normal fault) in the eastern margin of the Kırşehir Block, salt domes, and the normal faults mainly in the sedimentary sequences on the Kırşehir Block which could be continued into the block (Figures 11 & 12).

The Çankırı Basin is floored by the NAOM and associated Upper Cretaceous units. Almost all lower Tertiary and Neogene units (Figure 2) display a wedge-like geometry thinning from north to south and from east to west (Figures 10 & 12b, c) and they are onlapping on the Kırşehir Block (Figure 13). The basin fill was found to be the thickest in the NE part of the basin (Figures 8, 10 & 12).

The youngest unit affected by the thrust faults is the Oligocene Güvendik Formation (Figure 10b),

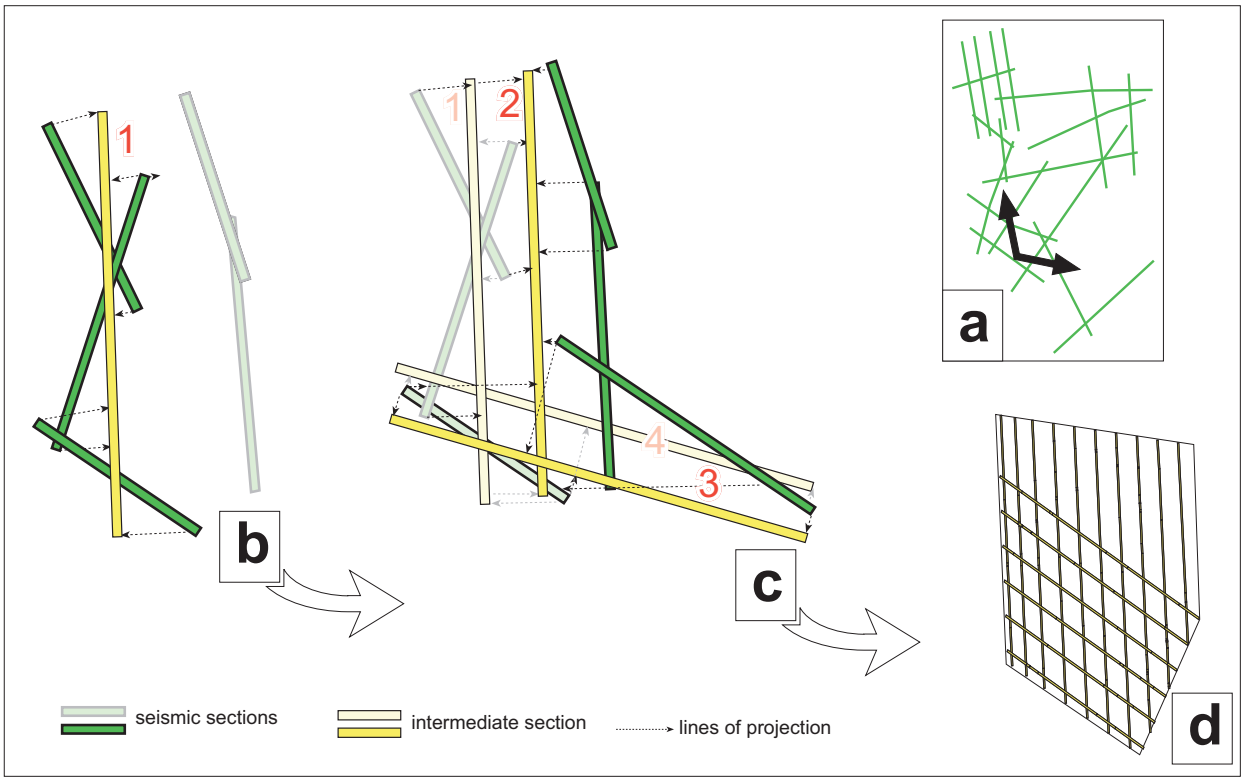

Figure 9. **(a)** Orientations of the seismic sections; arrows are the orientations of the intermediate sections that are used to generation of the fence diagram of the part of the Çankı Basin. **(b–c)** Procedure followed in construction of intermediate sections. After the first intermediate section is produced using the closest seismic sections **(b)**, then the next section is produced using another set closest to the second intermediate section. The previous seismic and intermediate sections including the transverse sections, produced with the same procedure (3–4 in **c**), are also used to smooth-out the previous sections, **(d)** final orientations of the intermediate sections.

which indicates that thrusting lasted at least until the Oligocene. These thrust faults were displaced by a number of normal faults oriented in various directions, namely NE–SW to NNE–SSW (Figures 10b & 12a, b). The eastern thrust belt is oriented parallel to a basement step of the Kırşehir Block, which may account for the accretion of these thrust sheets in this part of the basin (Figure 10b). The northern thrust faults have displaced the Middle Eocene to Oligocene İncik Formation and have affected the Middle to Upper Miocene units, resulting in folding at the tip lines of the faults (Çandır, Tuğlu, Süleymanlı, and Bozkır formations, Figure 2). The concentration of thrust faults and accretion of thrust sheets in the northern part of the basin may indicate indirectly that accretion is affected by a ramp formed at the northern tip of the Kırşehir Block. Unfortunately, its exact position could not be identified in the seismic sections.

The salt domes concentrate along a NNE–SSW line in the east central part of the model. Most of the salt domes arise from the top of the Early to Middle Eocene Kocaçay Formation (Tko, Figures 10 & 12) and affect Middle Miocene to Tortonian units (Figure 11), indicating that they were mobilized in post-Middle Eocene to Tortonian times.

Normal faults observed within the Middle Miocene to Tortonian units (Tç and Ttu) have the characteristics of dominant growth faults with thicker sediments on the downthrown side and thinner sediments on the upthrown side. Some of these normal faults display typical inversion structures (McClay 1989) (Figures 12c & 13).

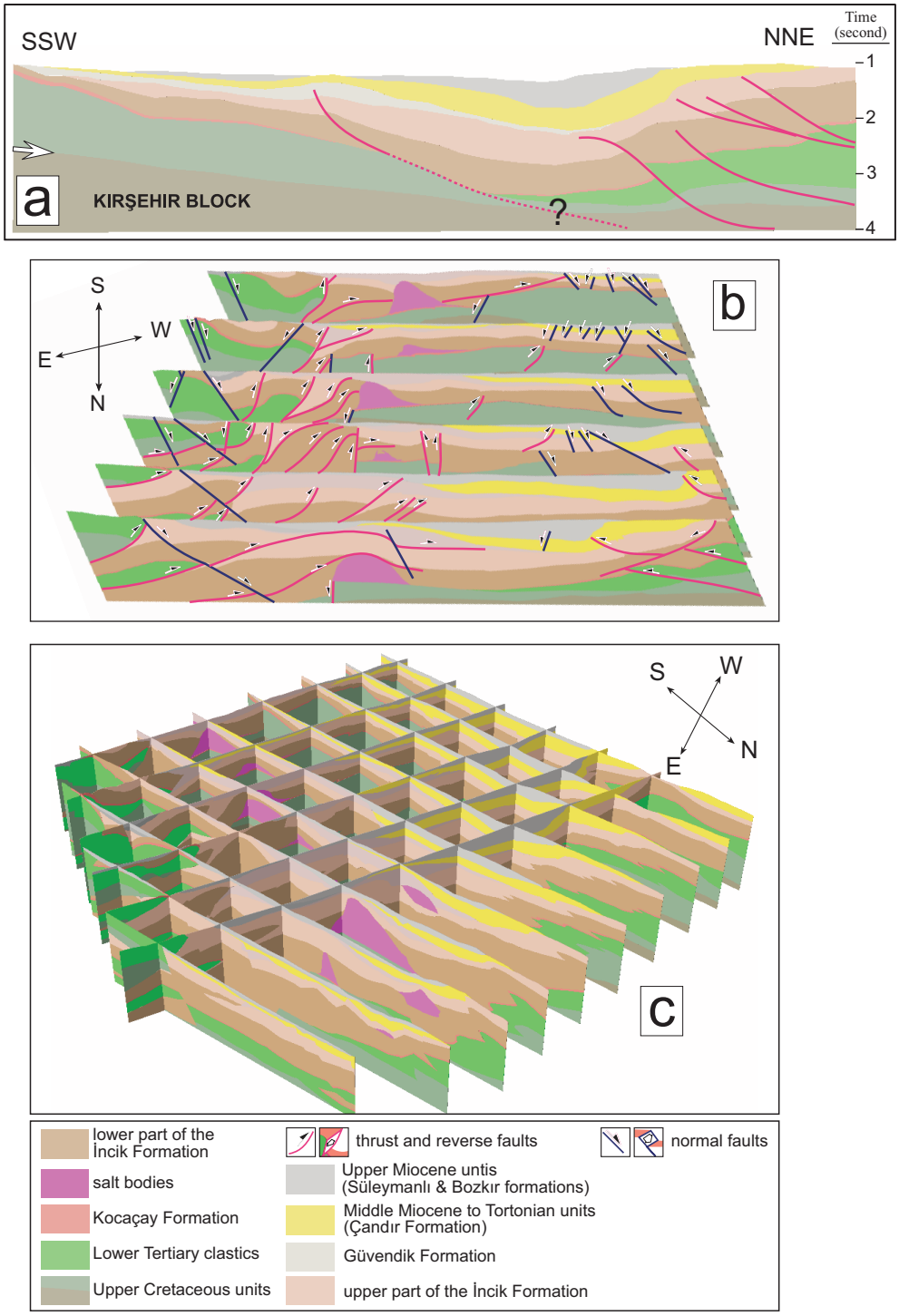

Figure 10. 3D models of the study area. **(a)** NNE–SSW cross-section obtained from the 3D model. Arrow shows the interface of a seismically distinct level within the basement. **(b)** E–W-trending fence diagrams of the basin that illustrate the mainly approximately N–S- oriented structures, **(c)** a complete fence diagram of the 3D model.

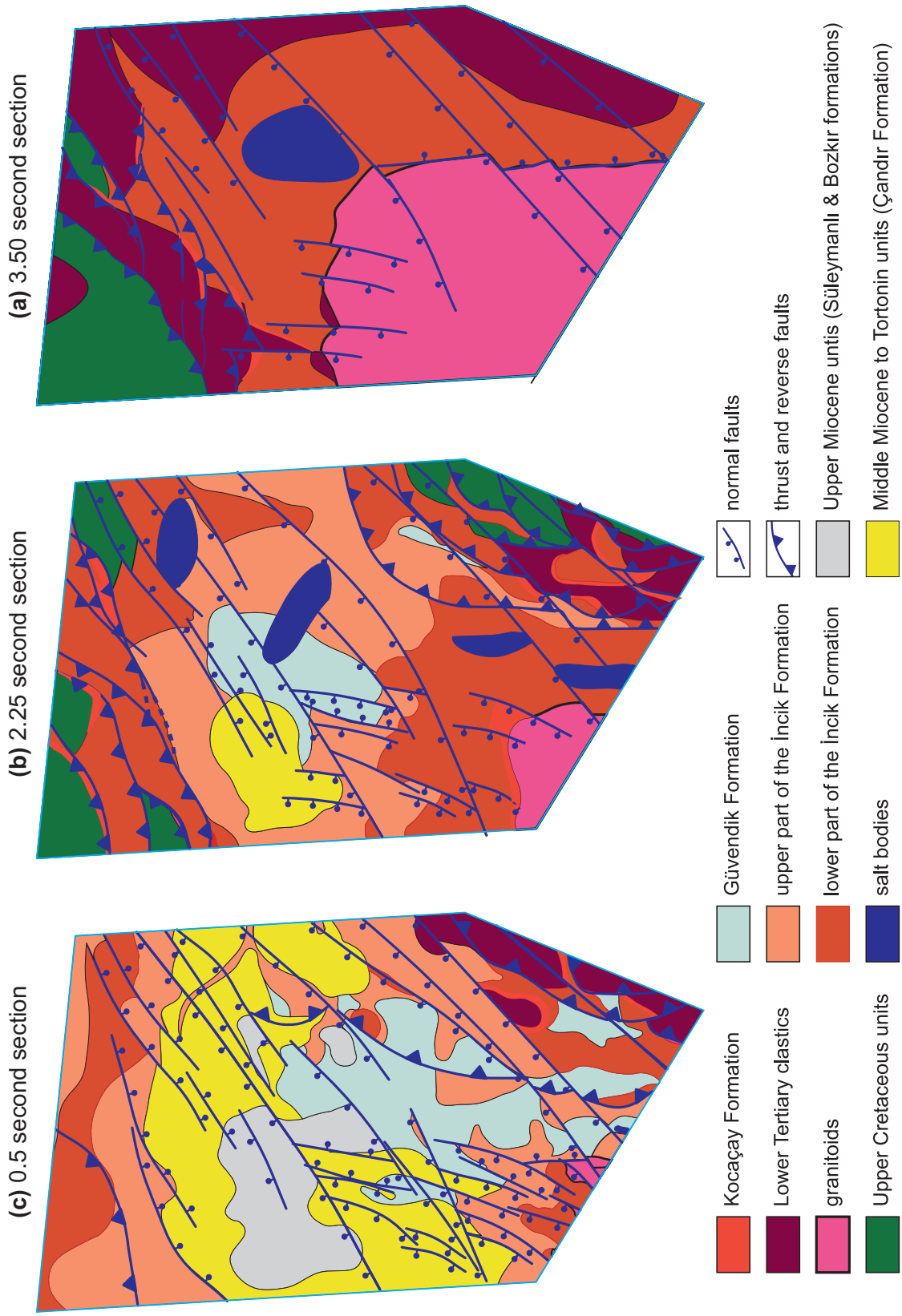

Figure 11. Time sections produced from the 3D model.

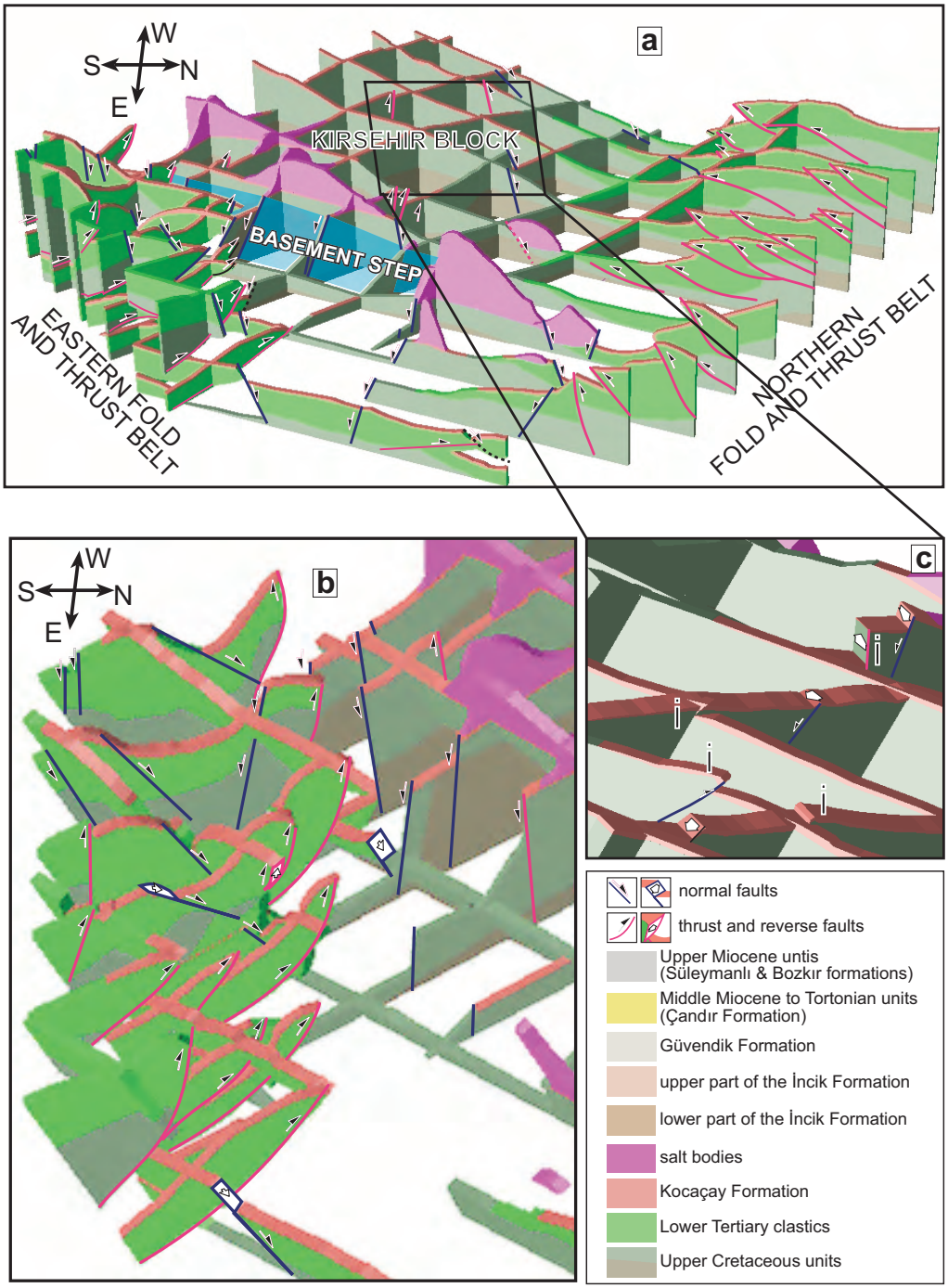

Figure 12. Fence diagrams of the 3D model area. The units above the Kocaçay Formation are stripped off. Note two thrust belts: one in the north and the other in the east. Note also the basement step, which is a normal fault in the eastern part of the Kırşehir Block **(a)**. Note also that the thrust faults **(b)** are displaced by a number of faults with normal off-set. These faults, in the seismic sections, appeared to be normal in nature however it does not exclude lateral movements which are actually observed on the surface. **(c)** Normal and reverse faults observed in the basement. Most of these reversed inverted growth faults. Examples are indicated with 'i' (see also Figures 12 & 13). **(c)** Blow-up image of the faults developed on the basement (look to NE).

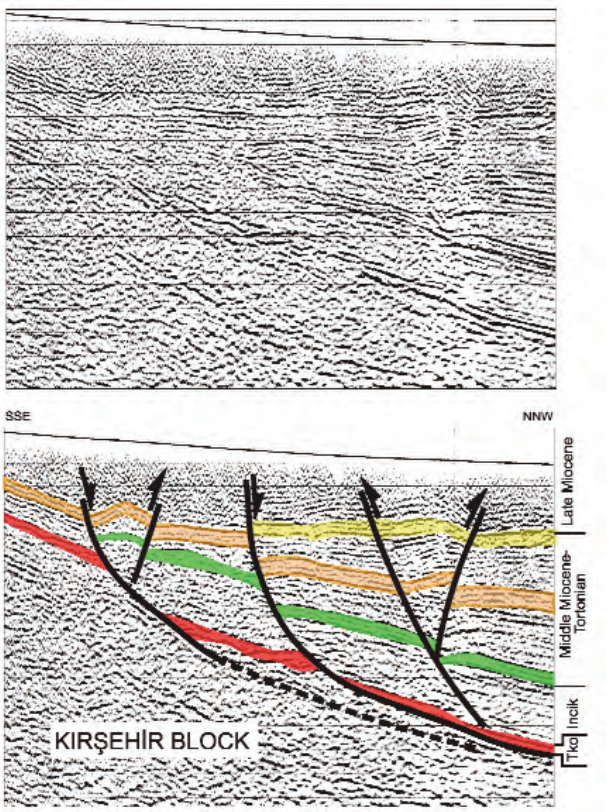

Figure 13. The original **(a)** and interpreted NNW–SSE-oriented seismic section **(b)**. Note that there is no thickening in the downthrown sides of the normal faults for the İncik Formation, while it is apparent for Middle Miocene to Tortonian units. Note also inverted nature of some these normal faults. Tko–Kocaçay Formation.

Discussion and Conclusions

29 lithostratigraphical units, 3 different deformation phases and related structures, 9 previously unrecognized and unmapped units were recognized and mapped in this study. In addition, the geological map, time section maps obtained from the 3D volume model and the images obtained from gravity data were integrated in a GIS and the results presented as different data layers. Overlaying the gravity map and the time sections allowed recognition of the vertical continuation and of the geometries of most of the units and the structures developed in the basin and on the Kırşehir Block. In addition, NE–SW-oriented faults, which are the vertical continuation of the Kızılırmak and Yağbasan-Faraşlı fault zones, were clearly traced from surface to the bottom of the seismic sections and their 3-D geometry was constructed in the volume models.

The wedge-like geometry of the lower Tertiary units indicates an asymmetry of the basin filling processes. On lap patterns in the sediments on the Kırşehir Block indicate migration of the depocenter towards the Kırşehir Block (Figure 13), which, in combination with their regressive character, syn-deformational geometries and provenance (discussed in Kaymakcı 2000) indicates that they were deposited during the development of the thrust belts.

In the overlay map produced from the processed gravity data and the 3.50s time section map, the basin in-fill and the positive gravity anomalies fit perfectly with each other (Figure 11a). In addition, the salt bodies, especially in the northeastern part of the area, correspond to a gravity low. The relatively high NE–SW-trending gravity anomaly in the northern part of the Çankırı Basin corresponds to the northern thrust belt. The dextrally displaced gravity high in the southernmost part of the model area corresponds to the Yağbasan-Faraşlı Fault Zone (YFFZ in Figures 1c & 4), which is also recognized in the time sections (Figure 11).

The displacement of the thrust faults by normal faults and inversion of these normal faults indicates that the Çankırı Basin evolved during at least three different phases of deformation from Early Tertiary to recent. The earliest deformation phase is characterized by compressional thrusting from Late Paleocene to pre-Early to Middle Miocene time (pre-Burdigalian). This phase corresponds to deformation phase 2, discussed in Kaymakcı *et al.* (2001a, b, 2003a). The displacement of these thrust faults by normal faults indicates that the compressional deformation phase was followed by an extensional deformation phase. Inversion of the normal faults indicates a possible phase of compressional deformation after the extensional phase. Each of these deformation phases has been discussed in more detail in Kaymakcı *et al.* (2000, 2001b, 2003a).

Finally, integration of satellite and airborne remote sensing data, seismic sections, gravity and

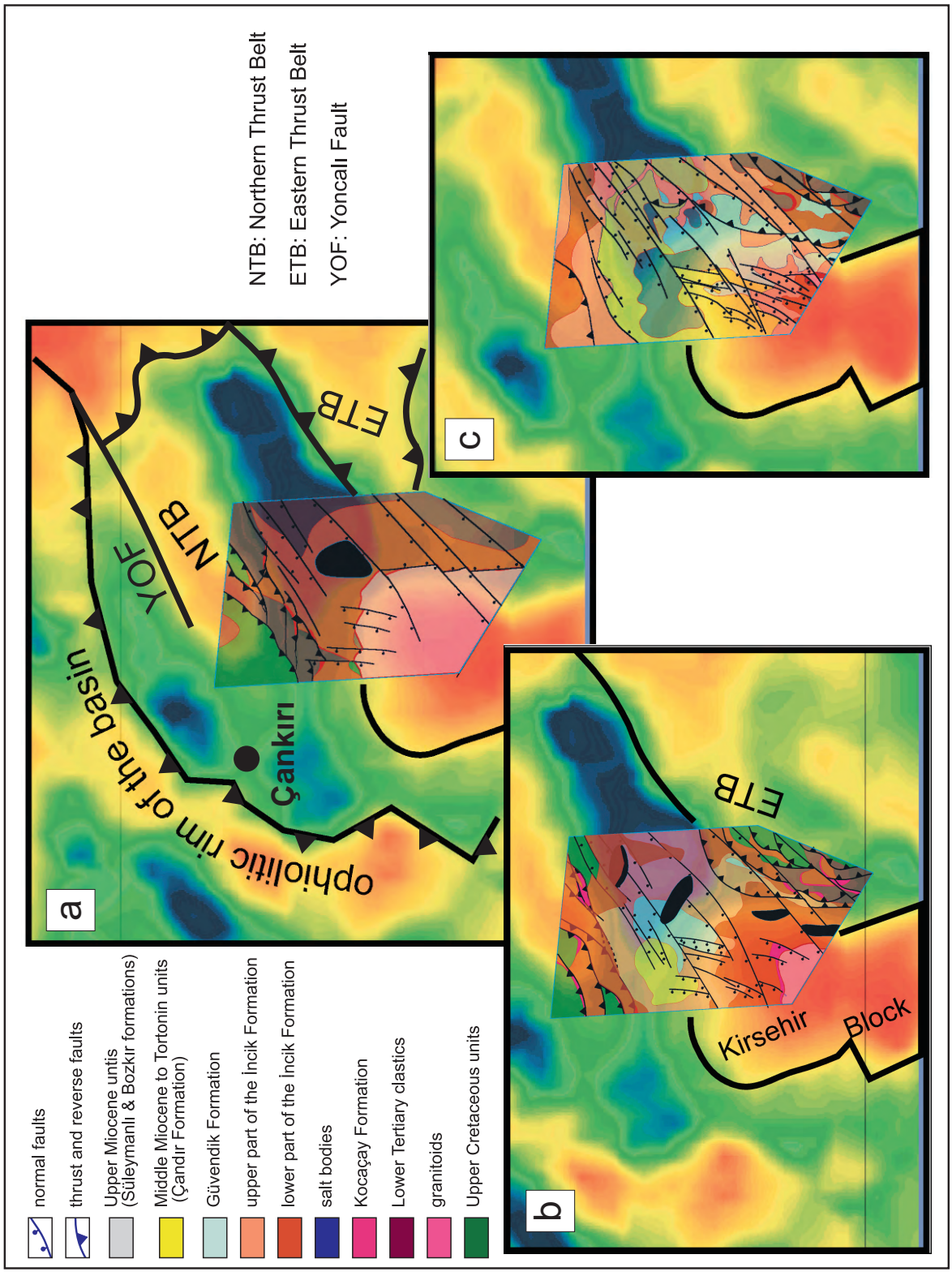

Figure 14. Overlay maps of gravity image and the time section maps (see Figure 11). Note the coincidence of outline of the Kırşehir Block (granitoids) in the gravity image and the 3.50s map **(a)**. Note also, alignment and positions of the salt bodies **(a, b)**.

field data facilitated construction of 3D model of the Çankırı Basin in order to better understand its 3D geometry and tectonosedimentary evolution and, in turn, the collisional history of the Sakarya Continent and the Kırşehir Block along the Izmir-Ankara-Erzincan Suture Zone.

Acknowledgements

We would like to Robert Hack for his help during the generation of 3D volumes. Dick Nieuwland critically reviewed and improved the manuscript. Turkish Petroleum Co. (TAPO) provided the seismic sections and supported field studies. John A. Winchester edited English of the final text.

References

Akyürek, B., Bilginer, E., Çatal, E., Dağer, Z., Soysal, Y. & Sunu, O. 1980. *Eldivan-Şabanőzű (Çankırı)-Hasayaz-Çandır (Kalecik-Ankara) dolayının Jeolojisi [Geology of Eldivan-Şabanőzű (Çankırı)-Hasayaz-Çandır (Kalecik-Ankara) Region]*. Mineral Research and Exploration Institute (MTA) of Tukey Report no. **6741** [in Turkish, unpublished].

Barka, A.A. 1992. The North Anatolian fault zone. *Annales Tectonicae* VI, 164–195,

Bartlett, W.L., Friedman, M. & Logan J.M. 1981. Experimental folding and faulting of rocks under confining pressure. Part IX. Wrench faults in limestone layers. *Tectonophysics* **79**, 255–277.

Chavez, P.S. Jr. & Kwarteng, A.Y. 1989. Extracting spectral contrast in Landsat Thematic Mapper Image data Using selective Principal Component Analysis. Photogrammetry. *Photogrammetric Engineering & Remote Sensing* **55**, 339–348.

Daily, M. 1983. Hue-saturation-intensity split-spectrum processing of Seasat Radar imagery. *Photogrammetric Engineering & Remote Sensing* **49**, 349–355.

Dellaloğlu, A.A., Tüysüz, O., Kaya, O.H. & Harput, B. 1992. *Kalecik (Ankara)-Eldivan-Yapraklı (Çankırı)-İskilip (Çorum) ve Devrez Çayı Arasındaki Alanın Jeolojisi ve Petrol Olanakları [Geology and Petroleum Potential of the Area Between Kalecik (Ankara)-Eldivan-Yapraklı (Çankırı)-İskilip (Çorum) and Devrez Çayı]*. Turkish Petroleum Coorporation (TPAO) Report no. **3194** [in Turkish, unpublished].

Dresen, G., 1992. Stress distribution and the orientation of Riedel shears. *Tectonophysics* **188**, 239–247.

Gillespie. A.R., Kahle, A.B. & Walker, R.E. 1986. Color enhancement of highly correlated images. I. Decorrelation and HIS contrast stretches. *Remote Sensing of Environment* **20**, 209–235.

Görür, N., Oktay, F.Y., Seymen, İ. & Şengör, A.M.C. 1984. Palaeotectonic evolution of the Tuzgölü basin complex, Central Turkey: Sedimentary record of a Neotethyan closure. *In*: Dixon, J.E. & Robertson, A.H.F. (eds), *The Geological Evolution of the Eastern Mediterranean*. Geological Society, London, Special Publications **17**, 467–482.

Grasso, D.N. 1993. Applications of the HIS color transformation for 1:24,000-scale Geological Mapping: a low cost SPOT alternative. *Photogrammetric Engineering & Remote Sensing* **59**, 73–80.

Hayden, R. 1982. The application of a colour transformation for the enhancement of multispectral images and for the combination of multispectral data. *Summaries: International Symposium on 'Remote Sensing of the Environment, Remote Sensing of Arid and Semi-Arid Lands, 3–9 November Cairo, Egypt*, p. 78.

Jackson, J. & Mckenzie, D. 1984. Active tectonics of the Alpine-Himalayan Belt between western Turkey and Pakistan. *Geophysical Journal International* **77**, 185–264.

Kaymakci, N. 2000. *Tectono-stratigraphical Evolution of the Çankırı Basin (Central Anatolia, Turkey)*. Ph.D Thesis, Geologica Ultraiectina. No. 190, Utrecht University Faculty of Earth Sciences, The Netherlands, ISBN 90-5744-047-4.

Kaymakci, N., White, S.H. & Van Dijk, P.M. 2000. Paleostress inversion in a multi-phase deformed area: kinematic and structural evolution of the Çankırı Basin (central Turkey): Part 1. *In*: Bozkurt, E., Winchester, J.A. & Piper, J. (eds), *Tectonics and Magnetism in Turkey and its Surroundings*. Geological Society, London, Special Publications **173**, 445–473.

Kaymakci, N., De Bruijn, H., White, S.H., Van Dijk, .M., Saraç, G. & Ünay, E. 2001a. Tectonic implications of the Neogene stratigraphy of the Çankırı basin with special reference to the Çandir locality (North-Central Anatolia, Turkey). *In*: Güleç, E, Begun, D.R. & Geraads, D. (eds), *Geology and Vertebrate Paleontology of the Miocene Hominoid Locality of Çandır*. Courier Forschungsinstitut Senckenberg **240**, 9–28.

Kaymakci, N., White, S.H., van Dijk, P.M. & Özçelik, Y. 2001b. Neogene tectonics of the Çankırı Basin (north Central Turkey). *Association of Turkish Petroleum Geologists Bulletin* **13**, 27–56.

Kaymakci, N., White, S.H. & van Dijk P.M. 2003a. Kinematic and structural development of the Çankırı Basin (Central Anatolia, Turkey). a paleostress inversion study. *Tectonophysics* **364**, 85–113.

Kaymakci, N., Duermeijer, C.E., Langereis, C., White, S.H. & van Dijk, P.M. 2003b. Oroclinal bending due to indentation: a palaeomagnetic study for the early Tertiary evolution of the Çankırı Basin (central Anatolia, Turkey). *Geological Magazine* **140**, 343–355.

Lavreau, J. 1992. De-Hazing Landsat Thematic mapper images. *Photogrammetric Engineering & Remote Sensing* **57**, 1297–1302.

Lynx Geosystems Incorporation 1997. Users Guide. http://www.lynxgeo.com/

McClay, R. K.R. 1989. Analogue models of inversion tectonics. *In*: Cooper, M.A & Williams, G.D (eds), *Inversion Tectonics*. Geological Society, London, Special Publications **44**, 41–62.

O`Leary, D.W., Friedman, J.D. & Pohn, H.A. 1976. Lineament, linear, lineation: some proposed new standards for old terms. *Geological Society of America Bulletin* **87**, 1463–1469.

Okay, A.I., Harris, N.B.W. & Kelley, S.P. 1998. Exhumation of blueschists along a Tethyan suture in northwest Turkey. *Tectonophysics* **284**, 275–299.

Özçelik, Y. 1994. *Tectono-stratigraphy of the Laçin Area (Çorum-Turkey)*. MSc. Thesis, Middle East Technical University, Department of Geological Engineering, Ankara, Turkey [unpublished].

Özçelik, Y. & Savun, C. 1993. *İskilip-Osmancık-Çorum-Sungurlu Arasındaki Alanın Jeolojisi ve Petrol Olanakları [Geology and Petroleum Patential of İskilip-Osmancık-Çorum-Sungurlu Area]*. Turkish Petroleum Coorporation (TPAO) Report no. **3290** [in Turkish, unpublished].

Park, R.G. & Jaroszwski, W. 1994. Craton tectonics, stress and seismicity. *In*: Hancock, P.L. (ed), *Continental Deformation*. Pergamon Press, 200–223.

Richard, J.A. 1993. *Remote Sensing Digital Image Analysis, An Introduction*. Springer Verlag, New York. 2nd Edition.

Robertson, A.H.F. & Dixon, J.E. (1984) Introduction: aspects of the geological evolution of the Eastern Mediterranean. *In*: Dixon, J.E. & Robertson, A.H.F. (eds), *The Geological Evolution of the Eastern Mediterranean*. Geological Society, London, Special Publications **17**, 1–74.

Robertson, A.H.F., Dixon, J.E., Brown, S., Collins, A., Morris, A., Pickett, E, Sharp, I. & Ustaömer, T. 1996. Alternative tectonic models for the Late Palaeozoic–Early Tertiary development of the Tethys in the Eastern Mediterranean region. *In*: Morris, A. & Tarling, D.H. (eds*)*, *Paleomagnetism of the Eastern Mediterranean Regions*. Geological Society, London, Special Publications **105**, 239–263.

Rojay, B. (1993) *Tectonostratigraphy and Neotectonic Characteristics of the Southern Margin of Merzifon-Suluova Basin (Central Pontides, Amasya)*. PhD Thesis, Middle East Technical University, Department of Geological Engineering, Ankara, Turkey [unpublished].

Rojay, B.F. 1995. Post-Triassic evolution of central Pontides: evidence from Amasya region, Northern Anatolia. *Geologica Romana* **31**, 329–350.

Şengör, A.M.C. & Yilmaz, Y. 1981. Tethyan evolution of Turkey: a plate tectonic approach. *Tectonophysics* **75**, 181–241.

Şengör, A.M.C., Yilmaz, Y. & Sungurlu, O. 1984. Tectonics of the Mediterranean Cimmerides: nature and evolution of the western termination of palaeo-Tethys. *In*: Dixon, J.E. & Robertson, A.H.F. (eds), *The Geological Evolution of the Eastern Mediterranean*. Geological Society, London, Special Publications **17**, 77–112.

Şengör, A.M.C., Şaroğlu, F. & Görür, N. 1985. Strike-slip deformation and related basin formation in zones of tectonic escape: Turkey as a case study. *In*: Biddle, K.T. & Christie-Blick, N. (eds), *Strike-Slip Deformation Basin Formation and Sedimentation*. Society of Economic Palaeontologists and Mineralogists, Special Publications **37**, 227–264.

Soha, J.M. & Schwartz, A.A. 1978. Multispectral histogram normalization contrast enhancement. *Proceedings, 5th Canadian Symposium on Remote Sensing*. Victoria, BC Canada, 86–93.

Sylvester, A.G. 1988. Strike-slip faults. Bulletin of the Geological Society of America 100, 1666–1703.

Taylor, M.M. 1974. Principal components color display of ERTS imagery. *Third Earth Resources Technology Satellite-1 Symposium, National Aeronautics and Space Administration Special Publication* no. **351**, 1877–1897.

Tüysüz, O. & Dellaloğlu, A.A. 1992. Çankırı Havzasının Ttektonik birlikleri ve Jeolojik evrimi [Tectonic units and geological evolution of the Çankırı Basin]. *Türkiye 9. Petrol Kongresi Kitabı*, 333–349.